

Kinetic Membrane Model of Outer Hair Cells I: Motile Elements with Two Conformational States

K. H. Iwasa

Bldg. 35A, Rm 1F242A

NIDCD, National Institutes of Health

Bethesda, Maryland 20892

date: 17 June 2019

running title: *Membrane Model of Outer Hair Cells*

keywords: *piezoelectricity, SLC26A5, equation of motion, turgor pressure*

Abstract

The effectiveness of outer hair cells (OHCs) in amplifying the motion of the organ of Corti, and thereby contributing to the sensitivity of mammalian hearing, depends on the mechanical power output of these cells. Electromechanical coupling in OHCs, which enables these cells to convert electrical energy into mechanical energy, has been analyzed in detail using isolated cells using primarily static membrane models. In the preceding reports, mechanical output of OHC was evaluated by developing a kinetic theory based on a simplified one-dimensional (1D) model for OHCs. Here such a kinetic description of OHCs is extended by using the membrane model, which has been used for analyzing in vitro experiments. The present theory predicts, for systems without inertial load, that elastic load enhances positive shift of voltage dependence of the membrane capacitance due to turgor pressure. For systems with inertia, mechanical power output also depends on turgor pressure. The maximal power output is, however, similar to the previous prediction of up to ~ 10 fW based on the 1D model.

1 Introduction

Outer hair cell (OHC) motility is essential for the sensitivity, frequency selectivity, and the dynamic range of the mammalian ear [1]. This motility is piezoelectric [2–5], based on a membrane protein SLC26A5 (prestin) [6]. This motility is driven by the receptor potential generated by the sensory hair bundle of the each cell. Even though the biological role of this motility has been confirmed by replacing it with its nonfunctional mutants [7], the mechanism, with which OHC motility plays this role, has not been fully clarified due to a number of puzzles.

One of them is the so called “RC time constant problem” due to the intrinsic electric circuit of the cell, which is expected to heavily attenuate the receptor potential at the operating frequencies of hair cells [8]. That is because, for the membrane potential to change, an electric current need to charge up or down the capacitor, consisting of the plasma membrane. To address this puzzle, a possibility has been explored that the cell was primarily driven by the extracellular voltage (cochlear microphonic), the attenuation of which with increasing frequency is less steep [9, 10]. However, the answer can be sought within the cell itself by examining the resistance (R) and the capacitance (C). Even though the membrane resistance can be overestimated in *in vitro* preparations [11], a lower membrane resistance does not lead to larger receptor potential even though it does reduce the RC time constant. Instead, a reduction of the membrane capacitance does increase the receptor potential at frequencies above the cell’s RC-corner frequency. While the movement of the motile molecule’s charge increases the membrane capacitance of the cell (nonlinear capacitance) under load-free condition, it is sensitive to mechanical load. It was found that elastic load can reduce the membrane capacitance [12]. Moreover, nonlinear capacitance can turn negative and eliminate the membrane capacitance altogether near resonance frequency in the presence of inertial load [13].

Another puzzle is the intrinsic transition rates of prestin. Nonlinear capacitance measured using the on-cell mode of patch clamp, which allows applying voltage waveforms without a low pass filter, rolled-off at ~ 15 kHz [14] at room temperature or at much lower frequencies [15]. Cell displacements elicited by voltage waveforms applied through a suction pipette showed frequency responses ranging from 6 to 80 kHz [16] or lower at 8.8 kHz [15]. Current noise spectrum from sealed patch formed on OHC showed relaxation time constant of 35 kHz, different from the value ~ 15 kHz for nonlinear capacitance, presumably reflecting a different mode of motion [17]. These observations indicate that those time constants reflect the mechanical relaxation time of each system rather than the intrinsic time constant of the motile molecules.

Previous theoretical efforts did address issue of high frequency response [18, 19] and the effect of elastic load [19]. However, these efforts did not consider the effect of load on the membrane capacitance, nor inertial load with an exception of a cochlear model [20] until the preceding reports [12, 13], which evaluated the effectiveness of OHCs by comparing the power output of OHC with energy

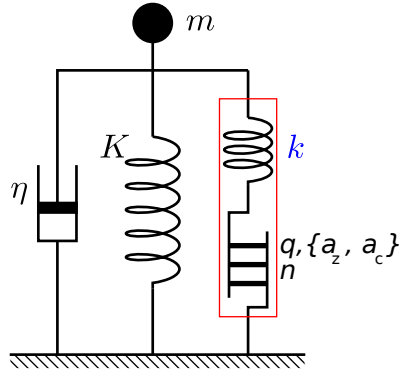


Figure 1: An OHC (red rectangle) is subjected to mechanical load, consisting of viscous η (left), elastic K (middle), and inertial m (top) components. The stiffness of the cell is k . The cell contains the motile element in its lateral membrane at density n . The motile element undergoes conformational transitions between the two states, with electric displacement q , and the mechanical displacements a_z and a_c respectively in the axial and circumferential directions (Fig. 2).

dissipation in the subreticular gap, essential for mechanoreception of the ear, in view of the importance of energy balance involving OHCs *in vivo* [21, 22]. Power output of OHCs was obtained by constructing the equation of motion of OHC with mechanical load. Nonetheless, the puzzles have not been fully clarified because these theoretical treatments include various approximations, which could affect the outcome, in addition to the paucity of experimental confirmations.

The present paper has twofold goals. One is to formulate a kinetic theory by extending the membrane model, which is more physical and has been used for analyzing quasi-static *in vitro* experiments yet simpler than shell model with more parameters [23]. This enables us to examine the limitations and accuracies of the 1D model that was used previously [12, 13]. It also allows to describe the effect of turgor pressure. The other goal is to prepare for extension to a more complex theory, in which the motile element has multiple states so that the effect of anion binding can be described [24–27]. Such an extension will be presented in the next report.

2 The system

Here we consider a system, in which an OHC has mechanical load, consisting of viscous, elastic, and inertial components (Fig. 1). It is not intended to simulate the organ of Corti, where OHCs are localized. Instead, this model system is intended to provide an OHC with a simplest possible environment so that its performance can be examined. The biological role of this cell could be inferred from this examination.

Let us assume that the cell maintains its characteristic cylindrical shape. Such a simplifying assumption could be justified for low frequencies, where inertial force is not significant compared with elastic force within the cell. The limit of the validity is examined later in Discussion, after experimental values for material properties are provided.

In addition, we consider movement of this cell in response to small fast

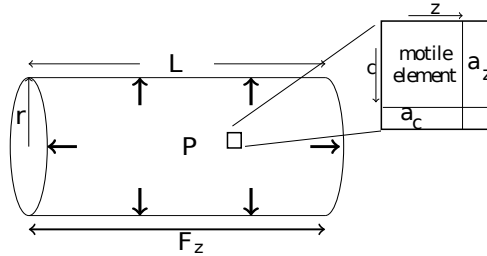


Figure 2: The membrane model of OHC. The cell body of an OHC is approximated by a cylinder of radius r and length L . Motile elements (upper right), which undergo area changes, a_z in the axial direction and a_c in the circumferential direction, are uniformly embedded in the cylindrical plasma membrane at density n .

changes in the membrane potential, from an equilibrium condition, ignoring metabolic processes that maintained the physiological condition. Changes in turgor pressure, if present, is assumed gradual and therefore has only a modulatory role. For this reason, the volume of the cell is assumed constant during voltage changes.

2.1 Electrical connectivity

Here we initially assume that the membrane potential of the cell is controlled by an extracellular electrode and an intracellular electrode with low impedance to facilitate the evaluation of the membrane capacitance. Later on, for evaluating power output of an OHC, the mechanotransducers at the hair bundle will be introduced because the receptor potential that drive the motile element in the OHCs depends on the membrane capacitance as well as the current source.

2.2 Static properties of OHC

First, consider an OHC in equilibrium. The shape of an OHCs is approximated by an elastic cylinder of radius r and length L . Small displacements of the cell can be described by constitutive equations [28],

$$d_1 \epsilon'_z + g \epsilon'_c = f_z + \frac{1}{2} r P, \quad (1a)$$

$$g \epsilon'_z + d_2 \epsilon'_c = r P, \quad (1b)$$

where ϵ'_z and ϵ'_c are respectively small elastic strains of the membrane in the axial direction and the circumferential direction. The quantities d_1 , d_2 , and g are elastic moduli of the membrane; P the internal pressure and f_z the axial tension due to an external force F_z , which can be expressed as $2\pi r f_z$. These elastic moduli assume orthotropy [29].

2.3 Axial stiffness

The material stiffness k in the axial direction and the axial elastic modulus κ of the cell are expressed as

$$k = \frac{2\pi r}{L_0} \kappa, \quad (2)$$

where L_0 is the resting length of the cell. The axial modulus κ is obtained as $\kappa = f_z/\epsilon'_z$ under constant volume condition $\epsilon'_v = \epsilon'_z + 2\epsilon'_c = \text{const.}$, eliminating ϵ'_c and rP from the constitutive equations (Eq. 1). It can be expressed as (See Appendix A).

$$\kappa = d_1 - g + d_2/4. \quad (3)$$

This axial stiffness of the cell is material stiffness without motile element, which would reduce the stiffness in a manner similar to “gating compliance.” [30, 31]

3 Motile element

Here we assume that each motile element undergoes transition between two states, compact (C) and extended (E). In the following, the fraction of the state is expressed in italic.¹

$$\mathbf{E}(\text{extended}) \rightleftharpoons \mathbf{C}(\text{compact}).$$

Unlike conventional description of molecular transitions, we do not assume that transitions between these states take place in accordance with “intrinsic” transition rates. Instead, we assume that transitions between these states are determined by the mechanical constraints in a manner similar to piezoelectricity.

To incorporate the motile element, let us assume that the total strain in the axial direction ϵ_z and the one in the circumferential direction ϵ_c consist of elastic components (ϵ'_z and ϵ'_c) and the contribution of motile elements. Each motile element undergoes electrical displacement q and mechanical displacements a_z and a_c (see Fig. 2) during the transition from state E to state C. If the motile elements are uniformly distributed in the lateral membrane at density n , the total strains in the two directions are then respectively expressed by [28]

$$\epsilon_z = \epsilon'_z + a_z n C, \quad (4a)$$

$$\epsilon_c = \epsilon'_c + a_c n C. \quad (4b)$$

¹The fraction of state C is used as the variable to describe the state of the motile element in this treatment so that this treatment can be extended to a system with motile elements, which undergo transitions between multiple states.

The constitutive equations are then re-written by

$$d_1\epsilon_z + g\epsilon_c - (a_z d_1 + a_c g)nC = f_z + \frac{1}{2}rP, \quad (5a)$$

$$g\epsilon_z + d_2\epsilon_c - (a_z g + a_c d_2)nC = rP. \quad (5b)$$

Notice that the internal pressure P now consists of two components, dependent on the activity of the motile element, and independent of it.

In the presence of external elastic load K , axial tension f_z can be expressed by

$$f_z = -K_e\epsilon_z, \quad (6)$$

where $K_e = KL_0/(2\pi r)$. Eqs. 5 and 6 lead to

$$\epsilon_z = -\frac{AnC - \mu\epsilon_v}{2(\kappa + K_e)}, \quad (7)$$

where $A = -(2d_1 - g)a_z + 2\mu a_c$ and $\mu = d_2/2 - g$ (See Appendix A). The quantity ϵ_v is the volume strain, which can be expressed as $\epsilon_z + 2\epsilon_c$ for the cylindrical cell for small strains.

Since the displacement of the cell that we are interested in is in the auditory frequency range, it is reasonable to assume the cell volume is constant. For this reason, we can regard ϵ_v as a variable representative of turgor pressure, which does not depend on the activities of the motile elements and can change only slowly responding to metabolic activity or osmotic pressure.

The axial displacement $z (= L_0\epsilon_z)$ of the cell and the total charge of the motile elements Q can be expressed respectively using C , the fraction of state C by ²

$$z = -\frac{L_0}{2(\kappa + K_e)} \cdot (AnC - \mu\epsilon_v), \quad (8a)$$

$$Q = -qNC, \quad (8b)$$

where N the total number of motile elements, i.e. $N = 2\pi r L_0 n$.

3.1 Boltzmann distribution

The fraction of state C in equilibrium should be given by a Boltzmann function

$$C_\infty = \exp[-\beta\Delta G_m]/(1 + \exp[-\beta\Delta G_m]), \quad (9)$$

$$\text{with } \Delta G_m = -q(V - V_0) - a_z f_z - (a_z/2 + a_c)rP \quad (10)$$

where ΔG_m is the energy difference (of state C from state E), V the membrane potential, $\beta = 1/k_B T$ with Boltzmann's constant k_B , and the temperature T .

²Since the fraction of state E was used in the previous reports, the resulting equations have the negative sign on A as well as on q . This alteration of the notations facilitates an extension of the present treatment into a system, where the motile elements undergo multiple state transitions.

The voltage V_0 determines the operating point. By substituting f_z and rP , we obtain (See Appendix A)

$$\Delta G_m = -q(V - V_0) + \frac{1}{4\kappa}[(A^2\hat{K} + \varphi a^2)nC - (\mu A\hat{K} - \varphi a)\epsilon_v], \quad (11)$$

where shorthand notations are

$$a = -(a_z + 2a_c), \quad (12a)$$

$$\hat{K} = K_e/(\kappa + K_e) = K/(k + K), \quad (12b)$$

$$\varphi = d_1 d_2 - g^2. \quad (12c)$$

The volume ϵ_v is due to turgor pressure P_t . Under the condition that the motile element is not active, $P_t = \epsilon_v \varphi / (2\kappa r)$.

4 Equation of motion

If $C = C_\infty$, i.e. the distribution of motor states are in equilibrium, the cell does not move. Suppose the membrane potential V changes abruptly, the cell exerts force $kAn(C_\infty - C)$, if the voltage change is small and deviation from the equilibrium is small. Here $k(= \kappa/L_0)$ is the material stiffness of the cell. The equation of motion can be expressed as

$$m \frac{d^2 z}{dt^2} + \eta \frac{dz}{dt} = kAn(C_\infty - C), \quad (13)$$

where C_∞ is the value of C , which satisfies Boltzmann distribution, for the given condition at time t . If the volume strain ϵ_v does not change, with the aid of Eq. 8a, this equation can be re-written in the form with the aid of Eq. 8a

$$m \frac{d^2 C}{dt^2} + \eta \frac{dC}{dt} = (k + K)(C_\infty - C), \quad (14)$$

using the variable C and stiffness (k and K) instead of elastic moduli (κ and K_e). This equation determines the rates of transitions between the two states because C is the only variable, given $C + E = 1$.

Notice that, the presence is the first term in Eq. 13 (and also in Eq. 14) is an assumption. In the absence of the inertial term, Eq. 13 has the typical form of a relaxation equation. Even though this equation appears reasonable at the moment $dz/dt = 0$, the presence of the inertial term may not be solidly justified. However, it will be shown later that this equation with the inertial term can be justified, being equivalent to the the equation that describes piezoelectric resonance if the deviation from equilibrium is small (See Discussion 8.3).

4.1 Small harmonic perturbation

Since one of the main functions of OHCs is to amplify small signal, the response of OHCs to small harmonic stimulation is of special interest. Assume that

the voltage consists of two parts, a constant term $\langle V \rangle$ and small sinusoidal component with angular frequency ω and amplitude v :

$$V(t) = \langle V \rangle + v \exp[i\omega t].$$

Then C and C_∞ should also have two corresponding components

$$C(t) = \langle C \rangle + c \exp[i\omega t], \quad (15)$$

$$C_\infty(t) = \langle C_\infty \rangle + c_\infty \exp[i\omega t], \quad (16)$$

and the first-order terms of the equation of motion turns into

$$[-(\omega/\omega_r)^2 + i\omega/\omega_\eta + 1]c = c_\infty, \quad (17)$$

with $\omega_r = \sqrt{(k+K)/m}$, $\omega_\eta = (k+K)/\eta$, and

$$c_\infty = \gamma[qv + \frac{nc}{2\kappa}(A^2\hat{K} + \varphi a^2)], \quad (18)$$

with $\gamma = \beta\langle C \rangle(1 - \langle C \rangle)$. Thus quantity c obeys the equation

$$[-(\omega/\omega_r)^2 + i\omega/\omega_\eta + \alpha^2]c = \gamma qv, \quad (19)$$

with $\alpha^2 = 1 + \gamma n(A^2\hat{K} + \varphi a^2)/(2\kappa)$.

4.1.1 Nonlinear capacitance

If we express corresponding changes in a similar manner, the charge variable can be expressed as $Q = nq\langle C \rangle + Nqc \exp[i\omega t]$, and nonlinear capacitance C_{nl} is given by

$$\begin{aligned} C_{nl} &= Re[Nqc/v], \\ &= Re \left[\frac{\gamma Nq^2}{\alpha^2 - \bar{\omega}^2 + i\bar{\omega}/\bar{\omega}_\eta} \right] \end{aligned} \quad (20)$$

where $Re[\dots]$ represents the real part because capacitance is charge transfer synchronous to voltage changes [12]. Here shorthand notations are introduced: $\bar{\omega} = \omega/\omega_r$, $\bar{\omega}_\eta = \omega_\eta/\omega_r$. The axial displacement z can be evaluated using Eqs. (8a) and (17).

5 Comparison with one-dimensional model

How the predictions of the membrane model differs from 1D models? In the following, the 1D model that was previously introduced [12, 13] is briefly restated to facilitate the comparison.

5.1 One-dimensional model

A 1D model has a single parameter k for the cell's elasticity and a single parameter a_1 for mechanical changes of the motile elements. For length changes z and charge transfer Q , the equation that correspond to Eqs. 8a can be written down [12],³

$$z = \frac{-a_1 k N C}{k + K} \quad (21a)$$

$$Q = -q N C, \quad (21b)$$

where C represents the fraction of the compact state, as in the membrane model. The comparison of Eqs. 8a and 21a suggest a_1 corresponds to A . The free energy difference ΔG_1 for the 1D model can be expressed by [12, 13]

$$\Delta G_1 = q(V - V_1) + a_1^2 N k \hat{K} C. \quad (22)$$

This energy difference ΔG_1 determines $C_\infty = \exp[-\beta \Delta G_1]/(1 + \exp[-\beta \Delta G_1])$ and contributes to the factor $\gamma_1 = \beta \langle C \rangle (1 - \langle C \rangle)$ in the equation of motion. The equation for c for the 1D model is

$$[-\bar{\omega}^2 + i\bar{\omega}/\bar{\omega}_\eta + \alpha_1^2]c = \gamma_1 q v, \quad (23)$$

with $\alpha_1^2 = 1 + \gamma_1 N a_1^2 k \hat{K}$.

5.1.1 Nonlinear capacitance

Since charge transfer is Nqc , nonlinear capacitance C_{1nl} is expressed by

$$C_{1nl} = Re \left[\frac{\gamma_1 N q^2}{\alpha_1^2 - \bar{\omega}^2 + i\bar{\omega}/\bar{\omega}_\eta} \right] \quad (24)$$

5.2 Correspondence between the two models

The charge transfer q is identical in the two models. The density n of the membrane model is related to N by $n = N/(2\pi r L_0)$. The relationship between the mechanical factors can be obtained by comparing Eq. 21a with Eq. 8a. These two equations together with Eq. 2 lead to the expression of unitary length change a_1

$$a_1 = \frac{A}{4\pi r \kappa}. \quad (25)$$

³The previous treatments used a variable P_ℓ , which corresponds to $P_\ell = 1 - C$. Thus the signs of a_1 and q are reversed in Eqs. 21 to keep the the signs of q and a the same as the previous treatments. In addition, $\tilde{K} = k\hat{K}$.

Table 1: Correspondence of parameters in the membrane model and in the 1D model.

1D model	membrane model
a_1	$A/(4\pi r\kappa)$
k	$2\pi r\kappa/L_0$
N	$2\pi rL_0n$
ΔG_1	ΔG_m
$\alpha_1^2 = 1 + \gamma_1 N a_1^2 k \hat{K}$	$\alpha^2 = 1 + \gamma n (A^2 \hat{K} + \varphi a^2)/(2\kappa)$

5.2.1 Dependence on elastic load and static turgor pressure

It might appear possible to formally replace C with $C - C_0$ in the 1D model to introduce the effect of turgor pressure. If we sort the resulting equations for the dependence on \hat{K} , we may find a correspondence

$$qV_1 \iff qV_0 - \frac{\varphi a}{4\kappa} \epsilon_v, \quad (26a)$$

$$a_1^2 N k (C - C_0) \hat{K} \iff \frac{A^2 n}{4\kappa} (C + \frac{\mu}{An} \epsilon_v) \hat{K}, \quad (26b)$$

leaving out a term $\varphi a^2 n C / (4\kappa)$ in Eq. 19.

Since $a_1^2 N k = A^2 n / (4\kappa)$, Eq. 26b might suggest correspondence $C_0 = -\mu \epsilon_v / An$, as if turgor pressure ϵ_v could be partially introduced through C_0 . Such a modification of Eq. 23, however, cannot be justified partially because there is no justification for including a term $a_1^2 N k C_0 \hat{K}$ in the free energy difference in the 1D model. In addition, $\varphi a^2 n C / (4\kappa)$, the term that was left out in the comparison, may not be small. If $\varphi > 0$, this term contributes the transition less sharp because it provides an additional negative feedback to the transition. Thus, such a modification predicts unreasonably sharper transitions.

6 Power output

The above analysis shows that membrane model leads to the equation for c , which is similar to the one derived for the 1D model. For example, the relation between z and c is the same for both cases because $a_1 k N / (k + K) = An / (\kappa + K_e)$. The difference of the two models originates only from γ and α^2 , which respectively differ from their counterpart γ_1 and α_1^2 (Table 1). For this reason, the expression for the 1D model will be used in the following with separate definitions for γ and α^2 for the membrane model and their counterparts γ_1 and α_1^2 for the 1D model.

Under physiological conditions, energy output from an OHC depends on the receptor potential v , which is generated by a relative change \hat{r} in the hair bundle resistance. This potential depends on the intrinsic circuit property of

the cell as well as charge movement due to changes in c , which can be expressed by [12]

$$v = \frac{-i_0 \hat{r} + i\omega Nqc}{\sigma + i\omega C_0}, \quad (27)$$

where i_0 is the steady state current, σ the conductance of the basolateral membrane, and C_0 the structural membrane capacitance of the hair cell.

The combination of Eqs. 19 and 27 can be written down in the form

$$\left[-\left(\frac{\omega}{\omega_r}\right)^2 + i\omega \left(\frac{1}{\omega_\eta} + \frac{\gamma Nq^2}{\sigma + i\omega C_0}\right) + \alpha^2 \right] c = \frac{\gamma i_0 q \hat{r}}{\sigma + i\omega C_0}. \quad (28)$$

For relatively high frequency, where ionic currents is overwhelmed by displacement current ωC_0 , we obtain

$$c = \frac{\gamma i_0 q \hat{r}}{i\omega C_0} \cdot \frac{1}{-\bar{\omega}^2 + i\bar{\omega}/\bar{\omega}_\eta + \alpha^2 + \zeta}, \quad (29)$$

with $\zeta = \gamma Nq^2/C_0$.

Energy output from an OHC has two components. One is elastic energy, $(1/2)kz^2$ per half cycle, which is recovered at the end of a cycle. The other is dissipative energy, $(1/2)\eta\omega|z|^2$ per half cycle, which results in power output W , which is given by

$$\begin{aligned} W(\omega) &= \frac{\eta\omega^2}{2\pi}|z|^2 \\ &= \frac{\eta}{2\pi} \left(\frac{k}{k+K}\right)^2 \cdot \left| \frac{\gamma a_1 Nq i_0 \hat{r}}{-\bar{\omega}^2 + i\bar{\omega}/\bar{\omega}_\eta + \alpha^2 + \zeta} \right|^2. \end{aligned} \quad (30)$$

Power generation in the membrane model is closely related to the 1D model [12, 13]. The only difference is from the expressions of free energy in the Boltzmann function, resulting in choosing the set γ and α^2 for the membrane model or γ_1 and α_1^2 for the 1D model.

6.1 Inertia-free condition

In the absence of the inertia term, the power output turns into

$$W(\omega) = \frac{\eta k^2}{2\pi(k+K)^2} \cdot \frac{(\gamma a_1 Nq i_0 \hat{r})^2}{(\omega/\omega_\eta)^2 + (\alpha^2 + \zeta)^2}, \quad (31)$$

which is a monotonically decreasing function of the frequency ω .

6.2 Near resonance

For the system with inertia, the power output has a peak

$$W^{(max)} \approx \frac{\gamma\zeta(a_1Ni_0\hat{r})^2\bar{\omega}_\eta^4}{\alpha^2 + \zeta} \cdot \frac{\eta k^2}{2\pi(k + K)^2C_0}, \quad (32)$$

at $\bar{\omega}^2 = \alpha^2 + \zeta - 1/(2\bar{\omega}_\eta^2)$. Since $\alpha^2 > 1$, such a peak exist if $\bar{\omega}_\eta < 1$. However, power production W is a decreasing function of the frequency ω for overdamped systems, where $\bar{\omega}_\eta$ is large.

These equations for power production are essentially the same as those for the 1D model, which has been studied previously [12, 13]. The difference is in the definition of α^2 and ζ even though these factors are similar.

Table 2: Parameter values of membrane model. e is the electronic charge. The parameter values of the motile element reflect that the extended state E is taken as the reference. (*): The experimentally obtained regular capacitance of an OHC is close to estimates based on the geometrical surface area with the standard value $\sim 1\mu\text{F}/\text{cm}^2$ for specific capacitance.

notation	definition	value used	refs.
d_1	axial modulus	0.046 N/m	[32]
d_2	circumferential modulus	0.068 N/m	[32]
g	cross modulus	0.046 N/m	[32]
a_z	axial area change	-4.5 nm ²	[28]
a_c	circumferential area change	0.75 nm ²	[28]
q	mobile charge	-0.8 e	
n	density of motile element	$9 \times 10^{15}/\text{m}^2$	[28]
r	radius	5 μm	[32]
L_0	cell length	25 μm	
C_0	regular capacitance	10 pF	(*)

7 Numerical examination

The membrane model and the 1D model lead to parallel expressions for mechanical and electrical displacements, which in turn lead to nonlinear capacitance and power output. The difference in the two stems from the difference in ΔG_m and ΔG_1 . Since the results of the 1D model have been previously elaborated, our focus is whether or not the membrane model leads to different results, using a set of parameter values that have been experimentally determined.

7.1 Nonlinear capacitance and factor γ

The factor γ , which contributes to α^2 and ζ , is affected by both turgor pressure and external elastic load through ΔG_m (See Eq. 10). This sensitivity is reflected in nonlinear capacitance in the low frequency limit (Fig. 3).

Increasing external elastic load broadens the voltage dependence as well as shifts the peak in the positive direction (Fig. 3A and B). An increase in turgor pressure, represented by ϵ_v , shifts the peak voltage of nonlinear capacitance in the positive direction. This effect of turgor pressure is consistent with earlier studies, both theoretical [2, 28] and experimental [2, 33, 34]. In addition, turgor pressure increases the sensitivity of nonlinear capacitance on the elastic load in both shifting the peak as well as broadening of the dependence (Fig. 3B). A contour plot of peak voltage shift summarizes the dependence on both turgor pressure and elastic load.

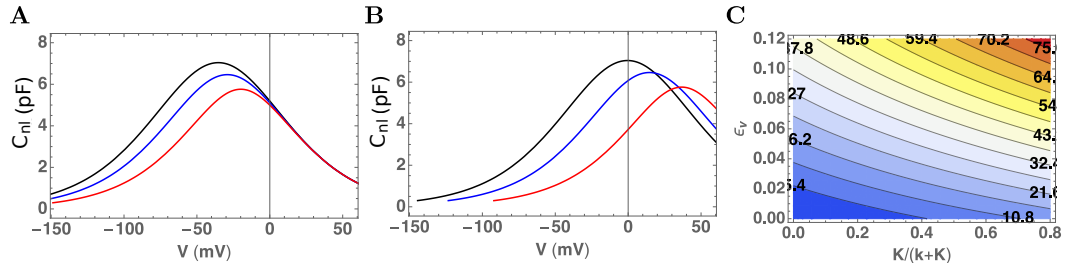


Figure 3: Nonlinear capacitance at low frequency. The volume strain ϵ_v are 0 for **A** and 0.10 for **B**. Traces represent elastic load K : 0 (black), 0.01 (blue), and 0.1 (red). **C**: Contour plot of peak voltage shift. The abscissa: $\hat{K}(= K/(k + K))$. The ordinate axis is volume strain ϵ_v , which represents static turgor pressure. Voltage shifts are color coded (blue: negative, red: positive) and the values (in mV) are shown in boldface letters in the plot.

7.2 Power output

Power output of an OHC has been described using the 1D model [12, 13]. Here we focus on the issue as to how the predictions of the membrane model compare with those of the 1D model for the given set of the parameters.

7.2.1 Inertia-free condition

Under inertia free condition, power output is a monotonic decreasing function of frequency as described by Eq. 31. The zero frequency asymptotes are $\gamma_m/(\alpha_m^2 + \zeta_m)$ for the membrane model and $\gamma_1/(\alpha_1^2 + \zeta_1)$ for the 1D model. The ratio of these zero-frequency asymptotes is plotted in Fig. 4A.

For high frequencies the power output declines proportional to $(1/\omega)^2$. The coefficients are proportional γ^2 . The ratio of the coefficient for the membrane model to that for the 1D model is plotted in Fig. 4B.

These ratios are very close to unity near $K = k$ (blue traces) and deviate significantly for larger elastic load at both ends of the membrane potentials. However, these deviations are not significant near the resting level of the membrane potential (Fig. 4).

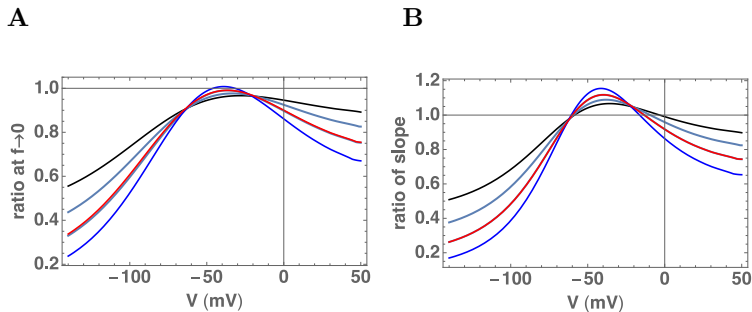


Figure 4: Ratio of coefficients for power output of the present membrane model to those of the 1D model. A: The ratio of power output of the membrane model to that of 1D model at zero frequency asymptote. B: The ratio at high frequencies. Traces correspond to, $K = 0.1k$ (blue), $0.5k$ (azure), k (blue), and $2k$ (red).

The previous analysis based on the 1D model indicates that the optimal elastic load K to for counteracting viscous drag is $K \approx k$ for physiological operating point near -50 mV [12].

The comparison shows that the power output of the membrane model is similar to that of the 1D model in the physiological membrane potential range. Outside of this voltage range, the membrane model predicts smaller power output than the 1D model. This smaller output is also dependent on the elastic load.

7.2.2 Near resonance

It has been shown with the 1D model that nonlinear capacitance is negative near resonance frequency and can make the total membrane capacitance negative (blue traces in Fig. 5A) and that the frequency of maximum power output (blue traces in Fig. 5B) is close to the frequency of zero capacitance in such cases (blue traces in Fig. 5C).

The membrane model predicts a similar relationship between the membrane capacitance and power output (red traces in Fig.5A–C are for $\epsilon_v = 0.065$). Power output predicted by the membrane model is slightly smaller than that of the 1D model for small load. However the membrane model predicts larger power output for large load K (Fig. 5D).

The difference between the two stems from the definitions of ΔG_m (Eq. 10) and ΔG_1 (Eq.22). For small K , the motile response of the membrane model is less sensitive than the 1D model because it has a negative feedback term that does not diminish with the load. However increased load K can reverse the

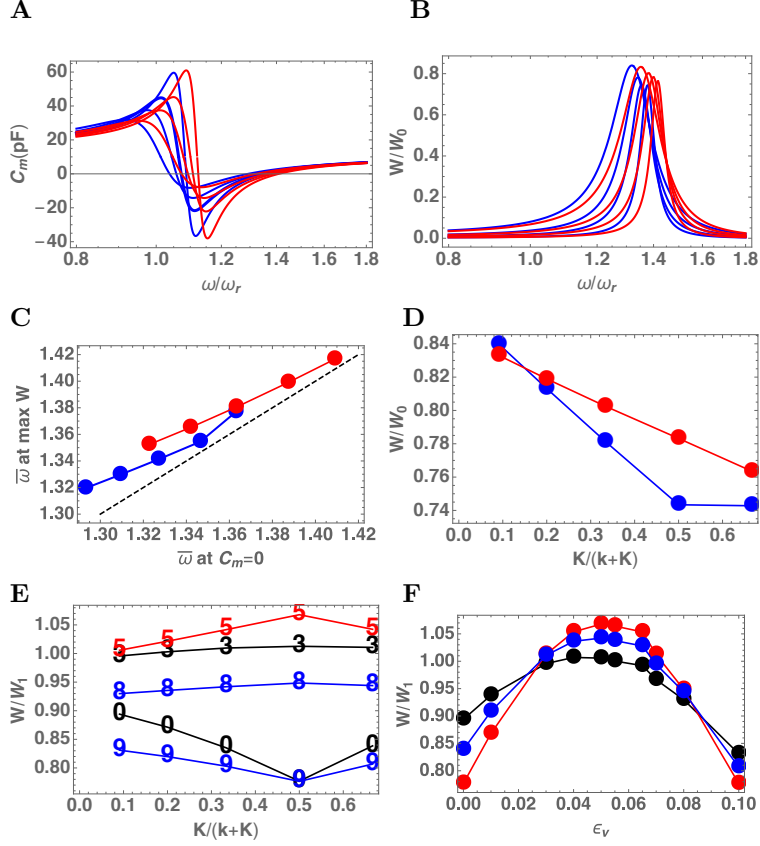


Figure 5: The membrane capacitance and the power output of an OHC. **A**: The membrane capacitance plotted against the reduced frequency ω/ω_r . The set of plots are generated by increasing the external elastic load K . The values of K correspond to $0.1k, 0.5k, k$, and $2k$ (from the left to right). Red: membrane model. Blue: 1D-model. **B**: Power output function plotted against frequency. The set of plots are generated by increasing K in a manner similar to **A**. **C**: Frequency of maximum power output against the frequency of zero membrane capacitance. The value of K corresponds to from the left to the right, $0.1k, 0.25k, 0.5k, k$, and $2k$. The broken line indicates equal frequency. **D**: Power output based on the membrane model (W_m : red) and on the 1D model (W_1 : blue) plotted against $\hat{K}(=K/(k+K))$. $W_0 = \eta(a_1 i_0 \hat{r})^2 / (2\pi C_0)$. **E**, **F**: Ratio of power output of the membrane model to that of 1D model. **E**: Dependence on the elastic load \hat{K} . The numbers in the ascending order correspond to $\epsilon_v = 0$ (labeled 0, black), 0.03 (3, black), 0.05 (5, red), 0.08 (8, blue), and 0.1 (9, blue). **F**: Dependence on volume strain ϵ_v . $\hat{K} = 0.05$ (red), 0.7 (Blue), 0.1 (black). In **A**–**D**, $\epsilon_v = 0.065$. The drag factor ω_η/ω_r is assumed to be 5 at $\hat{K} = 0$.

significance of negative feedback because an increase in the load K does not increase negative feedback in the membrane model as much as it does in the 1D model.

The ratio W_m/W_1 of power output predicted by the membrane model to

that of the 1D model depends on both turgor pressure and the elastic load (Fig. 5E, F). The ratio is larger than unity for $\epsilon_v = 0.05$ and maximizes at $\hat{K} = 0.5$, where it is about 1.07 (Fig. 5E). The ratio is lower at both larger and smaller values of ϵ_v , where ratio decreases between 0.8 and 0.9.

For every fixed value of the elastic load, the power output ratio has a broad maximum at $\epsilon_v = 0.05$ (Fig. 5F). The dependence on turgor pressure is sharpest for $\hat{K} = 0.5$, i.e. the stiffness of the elastic load is the same as the material stiffness of the OHC (Fig. 5F). The ratio is between 1.07 (at $\hat{K} = 0.5$) and about 0.8.

In the previous analysis based on the 1D model, estimated power output of an OHC was between 0.1 and 10 fW near resonance frequency [13]. The effectiveness of OHC under *in vivo* condition was estimated by evaluating a limiting frequency at which the power output of the OHC was equal to the viscous loss, assuming that the major contribution is from the gap between the tectorial membrane and the reticular lamina [22, 39, 40]. This frequency is constrained by two factors, resonance frequency and impedance matching: higher resonance frequency requires stiffer elastic load, which leads to poorer impedance matching for power transfer. This evaluation led to the limit of ~ 10 kHz if OHC is directly associated with the motion of the basilar membrane [13]. To support higher frequencies OHC needs to be associated to smaller elastic load and smaller mass, requiring multiple modes of motion in the organ of Corti [13]. The slightly larger ($\sim 7\%$) power output predicted by the membrane model leads to a slightly higher limiting frequency.

8 Discussion

It was assumed in the beginning that the cylindrical shape of the cell is maintained while the cell is driven by changes in the membrane potential and undergo deformation. First, the validity of this assumption is examined. A somewhat related issue is the magnitude of the internal drag. That is discussed next. That is followed by possible implications of turgor pressure dependence. In the last part, the comparison with standard piezoelectric resonance is discussed.

8.1 Limitation of validity

The conservation of the cylindrical shape of the cell during motion of the OHC requires that the elastic force of the membrane exceeds the inertial force of the internal fluid. Let x the amplitude of the end-to-end displacement of a cylindrical cell of radius r and length L . This condition can be expressed by

$$2\pi r \kappa \cdot \frac{x}{L} \gg \rho \pi r^2 x \cdot \omega^2 x, \quad (33)$$

where κ is the elastic modulus of the cell (in the axial direction), ρ the density of the internal fluid, ω the angular frequency. The inequality can be expressed

by defining a frequency ω_{bal} , at which these two factors are balanced, as

$$\omega \ll \omega_{\text{bal}} \equiv \sqrt{\frac{2\kappa}{\rho r x L}}. \quad (34)$$

This expression is intuitive in that a smaller displacement, a decrease in cellular dimension as well as an increase in the elastic modulus favor the elastic force over the inertial force.

The experimentally obtained value for $2\pi r \kappa$ is 510 nN per unit strain and it is reasonable to use the density of water 10^3 kg/m^3 for the density ρ . The radius r is $5 \mu\text{m}$ and the length L is $10 \mu\text{m}$ for a basal cell. If we assume the amplitude x is 1 nm, an approximate magnitude under *in vivo* condition, the limit can be expressed by the linear frequency

$$f_{\text{bal}} = 4 \times 10^6 \text{ Hz}, \quad (35)$$

about 40 times higher than about 100 kHz for high frequency mammals such as bats and dolphins. The condition is even more favorable for more apical cells because f_{bal} decreases with to the square root of $1/L$ whereas the best frequency decreases much steeper.

This means we can reasonably assume that relative motion of the internal fluid against the plasma membrane can be ignored and that the main mode of cell deformation is elongation and contraction while keeping the cylindrical shape.

8.2 The role of turgor pressure

The predicted dependence of power output of OHC on turgor pressure (Fig. 5D) raises a number of interesting questions. What is the range of turgor pressure *in vivo*? How much turgor pressure can change? Whether can it function as a control parameter of the cochlear function?

Power output has a plateau with respect to ϵ_v at about $\epsilon_v = 0.05$ (Fig. 5D), which corresponds to a static axial strain of $\epsilon_z = -0.018$ under load-free condition. This strain is about 36% of the maximum amplitude of electromotility (5% of the cell length). The corresponding turgor pressure is 0.14 kPa. It is probable that the physiological turgor pressure could be lower than this value as often the case for biological functions. Such an operating condition allows gain control by the parameters.

However, turgor pressure is not a simple control parameter of power output because changes in turgor pressure accompanies shifts of the operating voltage (see e.g. Fig. 3) even though its effect on the maximal power output is to up 20% (Fig. 5F).

8.3 Piezoelectric resonance

The derivation of the equation of motion (Eq. 17) may not appear legitimate in that it introduces the inertia term to a stochastic equation. However, it

turns out to be consistent with a standard expression for the admittance of a piezoelectric system.

The standard expression for the admittance Y_{pe} of a piezoelectric resonator can be [35]

$$Y_{pe}(\omega) = i\omega C_0 + \frac{1}{R + i[\omega L_p - 1/(\omega C_p)]}, \quad (36)$$

using an equivalent electric circuit with inductance L_p , and resistance R . That implies the correspondence to mechanical resonance system: $\omega_r^2 = 1/(C_p L_p)$ and $\omega_\eta = 1/(R C_p)$, leading to

$$Y_{pe}(\omega) = i\omega C_0 + \frac{iC_p}{i\omega/\omega_\eta + 1 - (\omega/\omega_r)^2}. \quad (37)$$

Eq. 37 is equivalent with Eq. 19 because $Y_{nl} = i\omega Nqc$ and the zero-frequency limit indicates $C_p = \gamma nq^2$ and $\alpha = 1$, which corresponds to $K = 0$ since the external spring does not exist for the piezoelectric element.

This comparison also illustrates a limit of validity for the equation of motion (Eq. 17). While Eq. 37 for standard piezoelectricity does not depend on the operating point, Eq. 19 for OHC does through the linearization near the equilibrium condition though the factor $\gamma (= \beta \langle C \rangle (1 - \langle C \rangle))$. The equation of motion Eq. 17 is valid only within a small range of the membrane potential, in which linearization can be justified.

9 Conclusions

The membrane model predicts nonlinear capacitance, cell displacement, and power output of OHCs relevant to *in vivo* conditions. In addition, these predictions are testable by *in vitro* experiments.

Nonlinear capacitance is sensitive to both turgor pressure and external elastic load. An increased elastic load reduces the peak height and broadens the voltage dependence of nonlinear capacitance. The peak voltage shifts in the positive direction with increasing turgor pressure and elastic load. That is intuitive because increasing internal pressure positively shifts the capacitance peak.

Power output depends on turgor pressure. The optimal power output is expected at $\epsilon_v = 0.05$ and $\hat{K} = 0.5$. Under this condition, maximal power output is about 7 % higher than the previous estimate based on the 1D model. However, the dependence of power output on turgor pressure is not large. The deviations from the predictions of 1D model do not exceed 20 %.

The membrane model confirms the main predictions of the 1D model: A single mode of vibration of organ of Corti can be supported up to about 10 kHz but to cover the entire auditory range cannot be supported without multiple modes of motion in the cochlear partition [13]. This prediction appears consistent with recent observations with optical techniques in general [36, 37],

and in particular with the presence of “hot spots” [38] of displacement around OHCs identified with optical coherence tomography (OCT) technique.

Acknowledgments

The author thanks Dr. Richard Chadwick for discussion. This research was supported in part by the Intramural Research Program of the NIH, NIDCD.

References

1. Liberman, M. C., J. Gao, D. Z. He, X. Wu, S. Jia, and J. Zuo, 2002. Prestin is required for electromotility of the outer hair cell and for the cochlear amplifier. *Nature* 419:300–304.
2. Iwasa, K. H., 1993. Effect of stress on the membrane capacitance of the auditory outer hair cell. *Biophys. J.* 65:492–498.
3. Mountain, D. C., and A. E. Hubbard, 1994. A piezoelectric model of outer hair cell function. *J. Acoust. Soc. Am.* 95:350–354.
4. Gale, J. E., and J. F. Ashmore, 1994. Charge displacement induced by rapid stretch in the basolateral membrane of the guinea-pig outer hair cell. *Proc. Roy. Soc. (Lond.) B Biol. Sci.* 255:233–249.
5. Dong, X. X., M. Ospeck, and K. H. Iwasa, 2002. Piezoelectric reciprocal relationship of the membrane motor in the cochlear outer hair cell. *Biophys. J.* 82:1254–1259.
6. Zheng, J., W. Shen, D. Z.-Z. He, K. B. Long, L. D. Madison, and P. Dallos, 2000. Prestin is the motor protein of cochlear outer hair cells. *Nature* 405:149–155.
7. Dallos, P., X. Wu, M. A. Cheatham, J. Gao, J. Zheng, C. T. Anderson, S. Jia, X. Wang, W. H. Y. Cheng, S. Sengupta, D. Z. Z. He, and J. Zuo, 2008. Prestin-based outer hair cell motility is necessary for mammalian cochlear amplification. *Neuron* 58:333–339.
8. Housley, G. D., and J. F. Ashmore, 1992. Ionic currents of outer hair cells isolated from the guinea-pig cochlea. *J. Physiol.* 448:73–98.
9. Dallos, P., and B. N. Evans, 1995. High-frequency outer hair cell motility: corrections and addendum. *Science* 268:1420–1421.
10. Mistrík, P., C. Mullaley, F. Mammano, and J. Ashmore, 2009. Three-dimensional current flow in a large-scale model of the cochlea and the mechanism of amplification of sound. *J R Soc Interface* 6:279–291.

11. Johnson, S. L., M. Beurg, W. Marcotti, and R. Fettiplace, 2011. Prestin-driven cochlear amplification is not limited by the outer hair cell membrane time constant. *Neuron* 70:1143–1154.
12. Iwasa, K. H., 2016. Energy Output from a Single Outer Hair Cell. *Biophys. J.* 111:2500–2511.
13. Iwasa, K. H., 2017. Negative membrane capacitance of outer hair cells: electromechanical coupling near resonance. *Sci. Rep.* 7:12118.
14. Gale, J. E., and J. F. Ashmore, 1997. An intrinsic frequency limit to the cochlear amplifier. *Nature* 389:63–66.
15. Santos-Sacchi, J., and W. Tan, 2018. The Frequency Response of Outer Hair Cell Voltage-Dependent Motility Is Limited by Kinetics of Prestin. *J. Neurosci.* 38:5495–5506.
16. Frank, G., W. Hemmert, and A. W. Gummer, 1999. Limiting dynamics of high-frequency electromechanical transduction of outer hair cells. *Proc. Natl. Acad. Sci. USA* 96:4420–4425.
17. Dong, X., D. Ehrenstein, and K. H. Iwasa, 2000. Fluctuation of motor charge in the lateral membrane of the cochlear outer hair cell. *Biophys J* 79:1876–1882.
18. Spector, A. A., W. E. Brownell, and A. S. Popel, 2003. Effect of outer hair cell piezoelectricity on high-frequency receptor potentials. *J Acoust Soc Am* 113:453–461.
19. Rabbitt, R. D., S. Clifford, K. D. Breneman, B. Farrell, and W. E. Brownell, 2009. Power efficiency of outer hair cell somatic electromotility. *PLoS Comput Biol* 5:e1000444.
20. O Maoiléidigh, D., and A. J. Hudspeth, 2013. Effects of cochlear loading on the motility of active outer hair cells. *Proc. Natl. Acad. Sci. USA* 110:5474–5479.
21. Ramamoorthy, S., and A. L. Nuttall, 2012. Outer hair cell somatic electromotility in vivo and power transfer to the organ of Corti. *Biophys J* 102:388–398.
22. Wang, Y., C. R. Steele, and S. Puria, 2016. Cochlear Outer-Hair-Cell Power Generation and Viscous Fluid Loss. *Sci. Rep.* 6:19475.
23. Spector, A., W. E. Brownell, and A. S. Popel, 1999. Nonlinear active force generation by cochlear outer hair cell. *J. Acoust. Soc. Am.* 105:2414–2420.

24. Oliver, D., D. Z. He, N. Klocker, J. Ludwig, U. Schulte, S. Waldegger, J. P. Ruppersberg, P. Dallos, and B. Fakler, 2001. Intracellular anions as the voltage sensor of prestin, the outer hair cell motor protein. *Science* 292:2340–2343.
25. Tunstall, M. J., J. E. Gale, and J. F. Ashmore, 1995. Action of salicylate on membrane capacitance of outer hair cells from the guinea-pig cochlea. *J. Physiol.* 485.3:739–752.
26. Homma, K., and P. Dallos, 2011. Evidence That Prestin Has at Least Two Voltage-dependent Steps. *J Biol Chem* 286:2297–2307.
27. Santos-Sacchi, J., and L. Song, 2014. Chloride-driven electromechanical phase lags at acoustic frequencies are generated by SLC26a5, the outer hair cell motor protein. *Biophys J* 107:126–133.
28. Iwasa, K. H., 2001. A two-state piezoelectric model for outer hair cell motility. *Biophys. J.* 81:2495–2506.
29. Tolomeo, J. A., and C. R. Steele, 1995. Orthotropic piezoelectric properties of the cochlear outer hair cell wall. *J. Acoust. Soc. Am.* 97:3006–3011.
30. Howard, J., and A. J. Hudspeth, 1988. Compliance of the hair bundle associated with gating of mechanoelectrical transduction channels in the bullfrog’s saccular hair cell. *Neuron* 1:189–199.
31. Iwasa, K. H., 2000. Effect of membrane motor on the axial stiffness of the cochlear outer hair cell. *J. Acoust. Soc. Am.* 107:2764–2766.
32. Iwasa, K. H., and M. Adachi, 1997. Force generation in the outer hair cell of the cochlea. *Biophys. J.* 73:546–555.
33. Kakehata, S., and J. Santos-Sacchi, 1995. Membrane tension directly shifts voltage dependence of outer hair cell motility and associated gating charge. *Biophys. J.* 68:2190–2197.
34. Adachi, M., M. Sugawara, and K. H. Iwasa, 2000. Effect of turgor pressure on outer hair cell motility. *J. Acoust. Soc. Am.* 108:2299–2306.
35. Ikeda, T., 1990. Fundamentals of Piezoelectricity. Oxford University Press, Oxford, UK.
36. Gao, S. S., R. Wang, P. D. Raphael, Y. Moayedi, A. K. Groves, J. Zuo, B. E. Applegate, and J. S. Oghalai, 2014. Vibration of the organ of Corti within the cochlear apex in mice. *J. Neurophysiol.* 112:1192–1204.
37. He, W., D. Kemp, and T. Ren, 2018. Timing of the reticular lamina and basilar membrane vibration in living gerbil cochleae. *eLife* 7.

38. Cooper, N. P., A. Vavakou, and M. van der Heijden, 2018. Vibration hotspots reveal longitudinal funneling of sound-evoked motion in the mammalian cochlea. *Nature Commun* 9:3054.
39. Allen, J., 1980. Cochlear micromechanics—A physical model of transduction. *J. Acoust. Soc. Am.* 68:1660–1670.
40. Hemmert, W., U. Dürig, M. Despont, U. Drechsler, P. Genolet, P. Vettiger, and D. Freeman, 2003. A life-sized, hydrodynamical, micromechanical inner ear. *In* A. Gummer, editor, *Biophysics of the Cochlea: from Molecules to Models*, World Scientific, 409–416.

Appendix A Derivations of ϵ_z and ΔG_m

The constitutive equations are given by Eqs. 5:

$$\begin{aligned} d_1\epsilon_z + g\epsilon_c - (a_z d_1 + a_c g)nC &= f_z + \frac{1}{2}rP, \\ g\epsilon_z + d_2\epsilon_c - (a_z g + a_c d_2)nC &= rP. \end{aligned}$$

For a cylindrical cell of length L and radius r , the cell volume is given by $V = \pi r^2 L$. For small length strains, ϵ_z in the axial direction and ϵ_c in the circumferential direction, the volume strain ϵ_v can be expressed by

$$\epsilon_v = \epsilon_z + 2\epsilon_c. \quad (\text{A.1})$$

By eliminating the circumferential strain ϵ_c from these equations, we obtain

$$(2d_1 - g)\epsilon_z + g\epsilon_v - 2(a_z d_1 + a_c g)nC = 2f_z + rP, \quad (\text{A.2a})$$

$$(g - \frac{d_2}{2})\epsilon_z + \frac{d_2}{2}\epsilon_v - (a_z g + a_c d_2)nC = rP. \quad (\text{A.2b})$$

By eliminating rP from Eqs. A.2, an expression for ϵ_z can be obtained. Then by replacing ϵ_z in Eq. A.2b with this expression, we obtain an expression for rP . They are

$$2\kappa\epsilon_z = -AnC + \mu\epsilon_v + 2f_z, \quad (\text{A.3a})$$

$$2\kappa rP = -\varphi anC + \varphi\epsilon_v - 2\mu f_z, \quad (\text{A.3b})$$

with short-hand notations

$$\begin{aligned} A &= -\nu a_z + 2\mu a_c, & \mu &= d_2/2 - g, \\ a &= -(a_z + 2a_c), & \nu &= 2d_1 - g, \\ \varphi &= d_1 d_2 - g^2. \end{aligned}$$

Notice here that the parameters A and a are defined such that they are positive. In the absence of the motile elements in the membrane Eq. A.3a is reduced to $f_z = -\kappa\epsilon_z$. This implies that κ is the axial elastic modulus. See Eqs. 2 and 3.

In the presence of external elastic load, $f_z = -K_e\epsilon_z$. Then Eqs. A.3 turn into

$$2(\kappa + K_e)\epsilon_z = -AnC + \mu\epsilon_v, \quad (\text{A.5a})$$

$$2\kappa rP = -(\mu A \hat{K} - \varphi a)nC + (\mu^2 \hat{K} + \varphi)\epsilon_v, \quad (\text{A.5b})$$

where $\hat{K} = K_e/(\kappa + K_e)$.

The axial stress f_z can then be expressed as

$$f_z = \frac{1}{2}\hat{K}(AnC - \mu\epsilon_v). \quad (\text{A.6})$$

The free energy ΔG_m of state C referenced from state E is given by

$$\Delta G_m = -q(V - V_0) - a_z f_z - (a_c + a_z/2)rP, \quad (\text{A.7})$$

where qV_0 is a constant term. Since $q < 0$ and $a_c + a_z/2 < 0$ ⁴, both depolarization and increased turgor pressure lead to a decrease of state C. By using Eqs. A.5b and A.6 to substitute rP and f_z in Eq. A.7, we obtain

$$\Delta G_m = -q(V - V_0) + \frac{1}{4\kappa}[(A^2\hat{K} + \varphi a^2)nC - (\mu A\hat{K} - \varphi a)\epsilon_v], \quad (\text{A.8})$$

which is Eq. 11 in the main text.

Appendix B Internal drag

For frequencies that satisfy $\omega \ll \omega_{\text{char}}$, the shape of an OHC can be approximated by a cylinder and the displacement of the cell could be virtually determined by the membrane elasticity alone as under static condition.

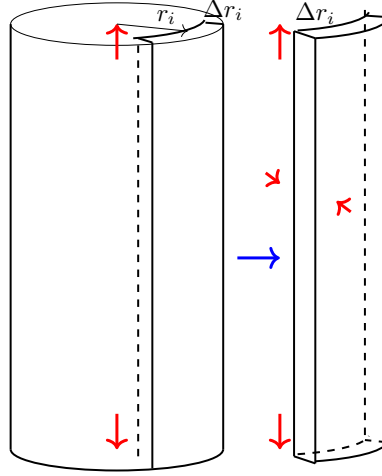


Figure B.1: Displacement of intracellular fluid.

Consider a part of a cylindrical layer of thickness Δr_i , the inner surface of which is located at distance r_i from the center. While the cell is elongating, the center of gravity moves toward inside due to constant volume condition, the internal fluid being incompressible. This layer elongates uniformly in the axial direction without slippage. The outer border moves more than the inner border does in the radial direction, but the direction of the movement is perpendicular to the surface and does not contribute to viscous drag. This description applies

⁴Unlike previous treatments, the state E is chosen here as the reference for the convenience of extension of this treatment to multi-state models.

throughout the cell interior. During the shortening of the cell, the reverse movement likewise does not involve slippage. For this reason, viscous drag must be virtually absent inside of an OHC, except for the lateral wall, the vicinity of the nucleus and the apical plate.

Appendix C Drag at the external surface

C.1 in vitro condition

Here we assume the roll-off frequency ω_f observed under load-free condition is determined by the drag at the external surface of OHCs and the cell's stiffness. Since it is expected that the drag coefficient η_e at the external surface increases with the length L of the cell exposed to the external fluid, it should be an increasing function of L .

The roll-off frequency ω_f under load-free condition is expressed by $\omega_f = k/\eta_e$. The axial stiffness of the cell k is related to the axial elastic modulus κ by $k = \kappa/L$. Thus we obtain an expression for drag coefficient:

$$\frac{\kappa}{\omega_f L} = \eta_e. \quad (\text{C.1})$$

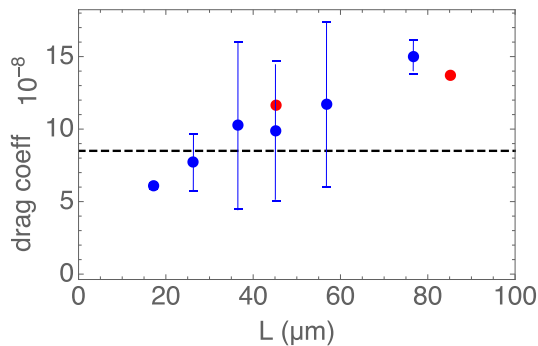


Figure C.1: Drag coefficient of the external surface of OHC. The drag coefficient η_e (in N·s/m) is plotted against cell length L . The value of κ is 510 nN per unit strain [32]. The data points are taken from Fig. 3A in ref. [16]. The two data points in red are taken from the same cell by changing the ratio of the cell body in the pipette. Error bars show standard deviations. Dashed line indicates the level of the Stokes drag of a sphere of $5\mu\text{m}$ radius.

Eq. C.1 can be examined with experimental roll-off frequency obtained in the microchamber configuration [16]. The order of magnitude of the drag coefficient is the Stokes drag of a $5\mu\text{m}$ sphere. In addition, the drag coefficient η_e appears to be an increasing function of the length L of the cell outside of the pipette, as expected.

This result is consistent with the hypothesis that conformational transitions of prestin is determined by mechanical constraints. It is also consistent with the analysis that internal drag is not significant.

C.2 *In vivo* condition

The space of Nuel, which surrounds the basolateral membrane of OHCs, undergoes displacement while OHCs move. If the displacement of this space parallels that of OHCs, an argument similar to the internal friction of OHCs could be made for the external friction. However, that is not the case for a number of reasons.

This space has structural elements other than OHCs. Deiters' cells, which connects OHCs to the basilar membrane, not only do not undergo active displacements the same as OHCs, their stiffness may not be the same. In addition, the phalangeal processes, which have stiff microtubule backbones, runs at an angle to OHCs, likely twisting the space when OHCs undergo displacement. Moreover, this space is continuous from the base to the apex, allowing fluid flow. Since the synchrony of OHC movement along the lateral axis should have a limited range, the volume of the extracellular space in a given segment may not be conserved.

For these reasons, an analogy to the internal surface does not apply to the external surface for the fluid motion. However, this drag may not be as large as under *in vitro* conditions.